ADVANCED FUNCTIONAL MATERIALS
www.afm-journal.de

A Novel Approach to Implementing Artificial Thalamic Neurons with Ferroelectric Transistors

*Andreas Grenmyr, Jiayuan Zhang, Jingxuan Sun, Kenta Moto, Stefan Wiefels, Seong-Ryong Koh, Detlev Grützmacher, and Qing-Tai Zhao**

Artificial thalamic neurons offer significant potential for medical treatment and neuromorphic computing applications. Their implementation with CMOS technology typically requires a large number of transistors and capacitors, leading to increased power consumption and reduced integration density. This work presents an artificial thalamic relay neuron using only five identical ferroelectric Schottky barrier field-effect transistors (Fe-SBFETs) based on silicon CMOS technology, forming a double inverter and a sensing transistor. The ambipolar switching behavior of Fe-SBFETs not only supports both excitatory and inhibitory synapses with a single device but also allows for the construction of inverters with just two identical transistors. The fabricated thalamic neuron exhibits leaky integrate-and-fire-or-burst (LIFB) functionality with self-resetting capabilities. The artificial neuron enables the device to generate spikes with a reset time of 10 µs, a spike frequency of 8.3 kHz, and an average energy loss of 40 pJ spike^{-1}. The successful implementation of artificial neurons is able to develop low-power, compact neural networks with relatively high operating frequencies.

1. Introduction

Artificial neurons are of great interest for both medical treatments and neuromorphic computing applications. The thalamus neuron, a central hub in the brain, plays a crucial role in sensory perception, motor control, regulation of consciousness and sleep, attention and cognitive functions, as well as emotional and pain perception. Beyond the basic science interest, the broad implications for society include the fact that 418 million disability-adjusted life years (DALYs) could be attributable to mental disorders in 2019 (16% of global DALYs). The economic burden associated with mental diseases is estimated at ≈5 trillion USD.[1] With 276 million DALYs, neurological disorders are the leading cause of disability.[2] The importance of the research on thalamic neurons in healthcare is underscored by its involvement in various neurological disorders, such as epilepsy, Parkinson's disease, and thalamic pain syndrome. Understanding and replicating thalamic functions can lead to advanced treatments and neural prosthetics, like deep brain stimulation, pain management, and even brain-machine interfaces.[3,4]

Developing artificial versions of the various biological neurons is essential since different neuron types working together are fundamental to neural systems.[4] Moreover, complex artificial neurons with stochastic properties can enable new probabilistic computing paradigms and perform complex tasks using basic circuits.[5] For neuromorphic computing, which seeks to emulate the brain's energy efficiency, artificial thalamus neurons can enhance sensory processing and decision-making algorithms, providing more accurate and efficient real-time responses in robotics and autonomous driving.[6–10]

In biology, neurons integrate stimuli from the dendrites (**Figure 1a**). When the neuron's membrane potential reaches a threshold, it triggers a spike in the axon hillock due to ion flow across the membrane, which then propagates along the axon to the synapse, transmitting the signal to the next neuron.[11,12] Thalamic neurons can generate continuous bursts of spikes without fully decaying to the resting state between spikes. These neurons can operate in two modes: a typical single spike or a burst when they are sufficiently depolarized.[13] Depending on the stimulus, the potential may drop below the resting voltage (hyperpolarization) before returning to rest or shifting from tonic to bursting.[14]

A. Grenmyr, J. Zhang, J. Sun, K. Moto, D. Grützmacher, Q.-T. Zhao
Peter Grünberg Institute (PGI-9)
Forschungszentrum Jülich
52428 Jülich, Germany
E-mail: q.zhao@fz-juelich.de

A. Grenmyr, J. Zhang, J. Sun
Faculty of Electrical Engineering and Information Technology
RWTH Aachen University
52074 Aachen, Germany

S. Wiefels
Peter Grünberg Institute (PGI-7)
Forschungszentrum Jülich
52428 Jülich, Germany

S.-R. Koh
Jülich Supercomputing Center (JSC)
Forschungszentrum Jülich
52428 Jülich, Germany

D. Grützmacher
Peter Grünberg Institute (PGI-10)
Forschungszentrum Jülich
52428 Jülich, Germany

The ORCID identification number(s) for the author(s) of this article can be found under https://doi.org/10.1002/adfm.202500512

DOI: 10.1002/adfm.202500512

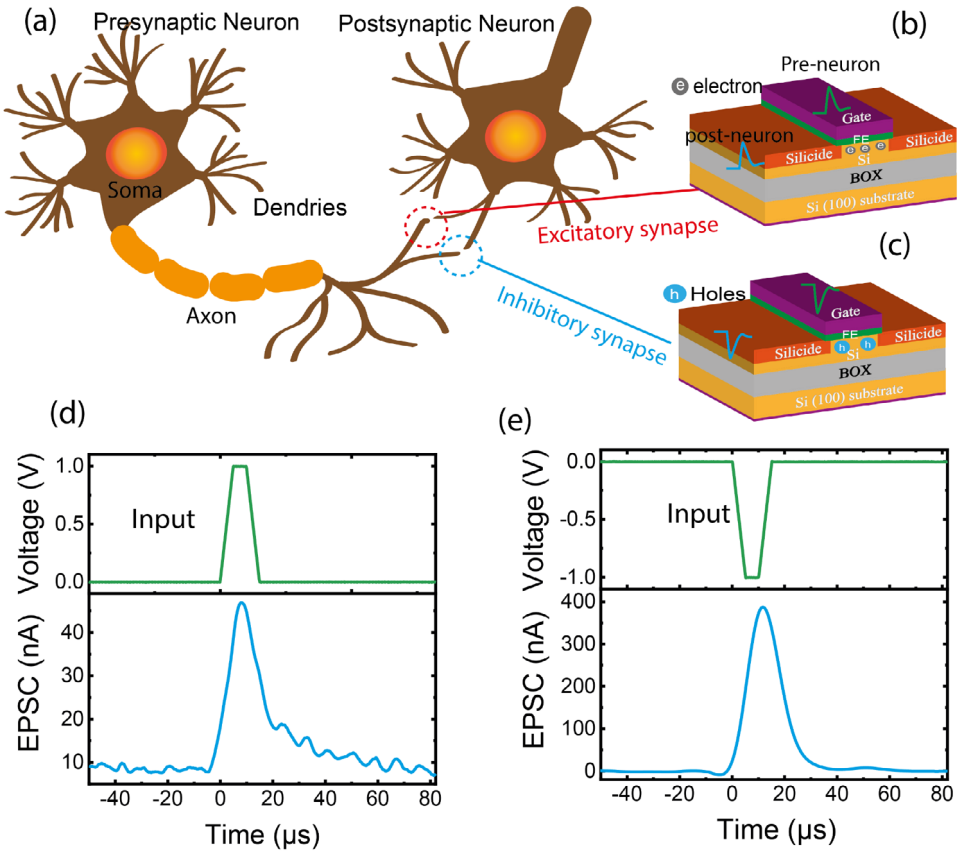

Figure 1. a) Illustration of biological neurons connected to synapses. The synapse can be imitated by Fe-SBFET as an excitatory synapse with electrons as the neurotransmitter b) or as an inhibitory synapse with holes as the neurotransmitter c). EPSC is generated from a single positive d) or a negative e) presynaptic voltage input pulse. The pulse generates excitatory electrons or inhibitory holes in the channel, enabling dual neurotransmitters, which results in the EPSC spike.

Thalamic neurons are considered gateways to the brain's cortex and are involved in information processing. Signals arriving in the brain can cause a burst of thalamic neuron activity, storing the signal during the burst and transmitting it to another brain region, functioning as a relay. Repeated stimuli can alter spiking behavior due to Ca^{2+} current activations.[6–8,13,15–17]

Current artificial neurons often require numerous transistors and capacitors. Charges generated by each input pulse are stored in a capacitor to integrate and release a spike.[18–20] An artificial thalamic relay neuron using CMOS technology consists of 19 transistors and 5 capacitors.[8] A recently reported neuron, fabricated with 180 nm CMOS technology, incorporates even more complex circuitry, including an integrator, comparator, one-shot pulse generator, and capacitors.[21] However, due to the difficulties of scaling capacitors and the high number of components, the CMOS neuron chip requires a large area, involves intricate fabrication processes, and consumes higher power. Some efforts have tried to reduce power consumption by utilizing double inverters, though the use of capacitors remains a limitation due to the poor scaling. Ferroelectric field-effect transistors (FeFETs) offer a promising solution for neuromorphic computing. Ferroelectric materials store polarization states when an electric field is applied, requiring minimal current to switch domains, making integration more effective by storing polarization rather than charge.[22] FeFETs also exhibit stochastic properties [23–25] though a reset pulse is needed after a spike, and the spike-to-integration regime ratio is small.[26,27]

This paper presents artificial thalamic neurons based on ferroelectric Schottky-barrier FET (Fe-SBFET) devices, eliminating the need for additional conventional transistors and capacitors. These neurons can self-reset within 10 μs. The unique ambipolar properties of Fe-SBFETs allow for inverters with a single device type.[28] The designed neuron consists of only 5 Fe-SBFET devices, demonstrating the characteristics of the biological thalamic relay neuron with low energy consumption and providing a more compact implementation using Fe-SBFETs.[3,4]

2. Artificial Neurons with Fe-SBFETs

2.1. Fe-SBFETs as Artificial Synapses

Figure 1a illustrates a biological neuron. Dendrites receive input from other neurons through synapses where the information is exchanged by inhibitory or excitatory neurotransmitters. If the excitatory synapse has stronger weights, it increases the potential at the neuron body (soma). However, the somatic potential decays if inhibitory synapses have stronger weights or no input is received.[29] Synapses store information in a neuromorphic

system, whereas neurons are necessary for network computations. Neurons exhibit certain distinctive features that artificial neurons replicate.

Artificial inhibitory and excitatory synapses can be realized by Fe-SBFETs utilizing holes or electrons as neurotransmitters, as illustrated in Figure 1b,c. We fabricated Fe-SBFET devices on Silicon-On-Insulator (SOI) substrates. The details of the fabrication process and device characterization are provided in the Experimental section and Figure S1 (Supporting Information). The characterization of the ferroelectric material is shown in Figure S1a (Supporting Information). The Schottky source and drain enable ambipolar switching, allowing the transistor to function as either an n-FET or p-FET, depending on the gate voltage (see Figure S1b, Supporting Information). Leveraging this ambipolar behavior, a single Fe-SBFET can serve as both inhibitory and excitatory synapses.

Here, we show the characteristics of a Fe-SBFET first as an artificial synapse by applying a voltage pulse on the gate (presynaptic neuron) and measuring the generated excitatory postsynaptic current (EPSC) at the source (postsynaptic neuron) with a voltage applied at the drain, as illustrated in Figure 1b,c. Figure 1d shows that applying a positive pulse on the gate creates an inversion channel with electrons, increasing the electron-driven conductance. Similarly, as shown in Figure 1e, a negative presynaptic spike is applied to the synapse, generating an EPSC due to the accumulation of holes in the channel. The short retention (decay) time shown in Figure 1d,e is caused by the low applied voltage (below the coercive field voltage) and the short pulse duration.[30] Under these conditions, only a fraction of the ferroelectric domains in the HZO layer become polarized. Once the voltage pulse is removed, subsequent depolarization results in a short retention time, which was also reported in our previous work for devices using a thicker SOI layer.[31]

The decay of the EPSC is shorter for holes than for electrons due to the lower absolute threshold voltage of the Fe-SBFET when operating as an n-FET compared to a p-FET, as shown in Figure S1b (Supporting Information). Consequently, the effective voltage for the positive pulse is higher and closer to the corresponding coercive field, leading to greater polarization and, therefore, a longer retention time. The long-term memory characteristics of the synapse are presented in Figures S1c,d (Supporting Information), showing that Fe-SBFET can operate as an excitatory synapse with electrons as neurotransmitters or as an inhibitory synapse with holes as neurotransmitters. They are similar to those of the Fe-SBFET device fabricated with a thicker SOI layer, as reported in a previous work.[31] Since this paper focuses on neuron functionality, we do not present them here.

2.2. Double Inverter as Leaky Integrate and Fire Neuron

We designed and fabricated a double inverter-based neuron using Fe-SBFETs with the structure as illustrated in **Figure 2a**. Figure 2b,c shows the cross-sectional transmission electron microscopy (TEM) images for the layer structures at the source/drain and the gate/channel regions, indicating very smooth interfaces between the layers. The $NiSi_2$ shows very good single crystalline quality. SiO_x interfacial layers are formed at the HZO/$NiSi_2$ and HZO/Si channel interfaces after processing. The ambipolar switching of Fe-SBFET enables us to fabricate an inverter block using two same Fe-SBFETs instead of requiring a conventional p-FET and an n-FET.[28] Figure 2d shows the circuit design of the neuron, which consists of three main building blocks: two series connected inverters and a single Fe-SBFET. An SEM image of the neuron circuit and the corresponding configurations is shown in the background before final metallization. $NiSi_2$ is used as the source/drain contacts for all transistors and as the first interconnect metal, while TiN is used as the gate contacts. A clear SEM image is displayed in Figure S2 (Supporting Information). The DC characteristics of these inverters are presented in Figure S3a,b (Supporting Information), while Figure S3c (Supporting Information) shows the response current for T5. Positive voltage pulses, V_{IN}, applied at the gates of Inverter 1, consisting of T1 and T2, correspond to excitatory neurotransmitter input (electrons) from an excitatory synapse. However, negative voltage pulses applied at the input generate inhibitory neurotransmitters (holes). Inverter 1 collects and sums up the input, functioning as the dendrite.

In the following, we first present the neuron functions produced by the double inverter using voltage as the output signal. Stimuli consisting of 30 short pulses (with a pulse width of 17 µs and an interval of 24 µs) are applied as input, as shown in Figure 2e. In Inverter 1, T1 operates as a p-FET in the on-state due to the large applied positive V_{DD} and low input voltage. Initially, T2 functions as an n-FET in the off-state, as its source is grounded and the gate receives a small positive pulse. As the number of positive pulses at V_{IN} increases, the remnant polarization across the ferroelectric layer builds up over time, enhancing the gate electric field in both T1 and T2. This leads to a decrease in the gate voltage of T1 and an increase in the gate voltage of T2, gradually depleting holes in T2. With further input pulses, hole depletion in the p-Si layer is followed by the formation of an electron inversion layer, transitioning T2 into n-channel operation. In contrast, the gate-source voltage of T1 becomes very small. As a result, the conductance of T2 increases, and T1 is switched off, causing the output voltage V_{OUT1} of Inverter 1 to shift from high to low. Therefore, the complementary operation of T1 as a p-FET and T2 as an n-FET enables the inverter function.

V_{OUT1} is applied as the input for Inverter 2. For a high V_{OUT1}, T4 is operating in the on-state as an n-FET, and T3 is off because of the high V_{DD} and V_{OUT1}. However, the decreased V_{OUT1} turns T4 gradually off and T3 gradually on, operating as a p-FET. This results in an increased output voltage of the Inverter 2 (V_{OUT2}). Effectively, the more applied input pulses lower V_{OUT1}, and it, in turn, switches V_{OUT2} from low to high voltage. When the input pulses stop, the V_{OUT2} decays for 2.3 ms due to the memory effects. This behavior is similar to how the membrane potential of the soma in the biological neuron reacts when an applied stimulus is removed. Therefore, V_{OUT2} simulates the membrane potential in the soma of a biological neuron.

One of the standard simplified models for describing the operational behavior of the neuron is the integrate-and-fire (IF) model [32] or with extensions such as the Morris-Lecar model or the leaky-integrate-and-fire (LIF) model.[33] The IF model describes a neuron that integrates input from the applied stimulus by increasing the potential of the neuron's membrane. The neuron generates a spike when the potential reaches a certain threshold, and the membrane potential is reduced to a resting value.

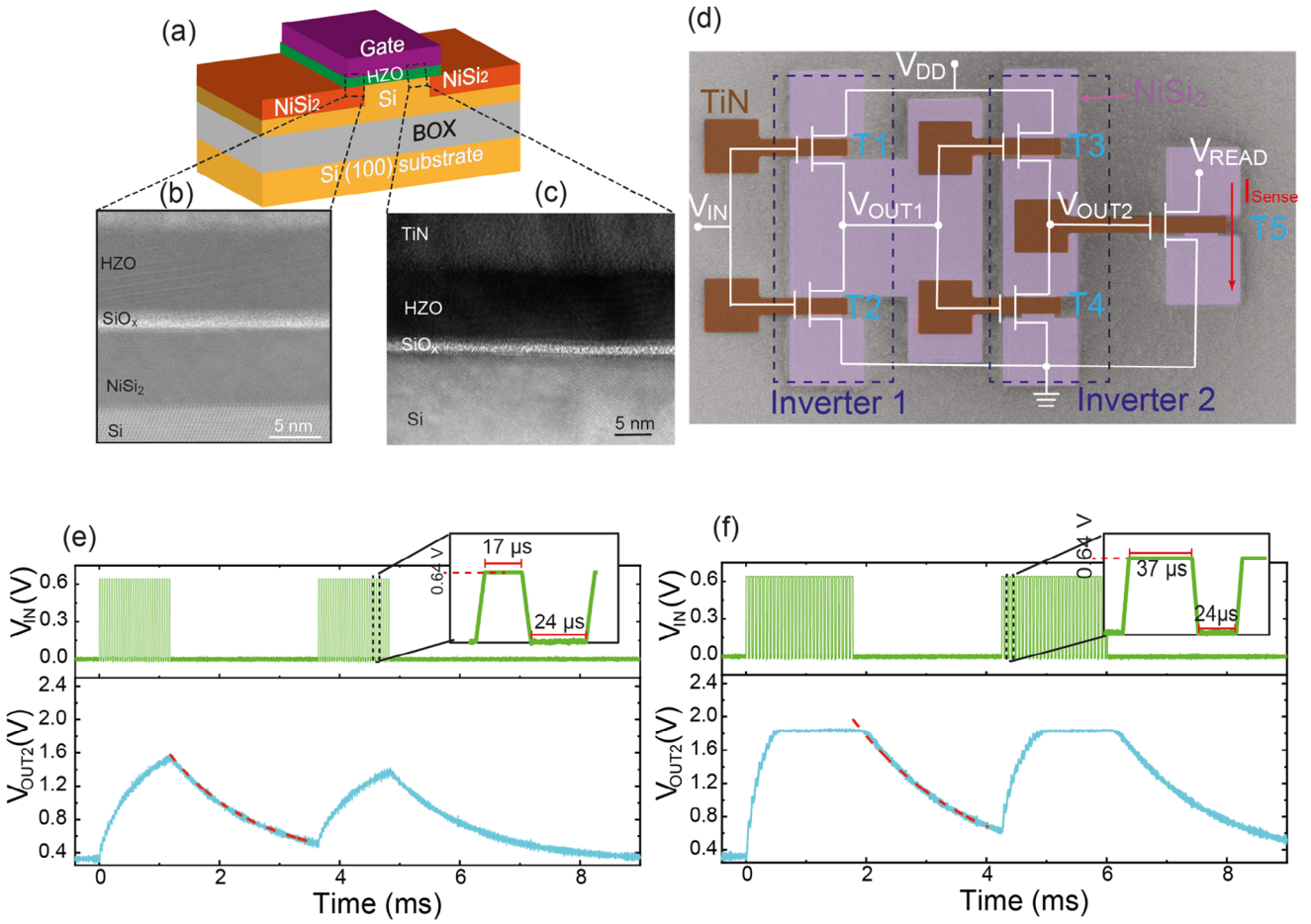

Figure 2. a) Structure of the Fe-SBFET. b) Cross-section TEM image showing the HZO/$NiSi_2$ stack at the source/drain, c) Cross-section TEM image for the TiN/HZO gate stack on top of the Si channel. Interfacial SiO_x layers are formed at both interfaces of HZO/$NiSi_2$ and HZO/Si. d)The designed circuit of the artificial relay neuron, with 2 inverters (T1-T4) and 1 sensing Fe-SBFET (T5). Positive (excitatory) pulses are applied to the gates of Inverter 1, and the output can be read from the output of Inverter 2 or the drain current of T5 (I_{Sense}). The background is the SEM image of the fabricated circuit before final metallization. e) Applying V_{IN} with 17 µs long pulses (top) generates an increased V_{OUT2}, corresponding to an increased somatic potential. V_{OUT2} decays with a decay time constant of 1.4 ms. f) Applying 37 µs long pulses (top) saturates the V_{OUT2}, resulting in a longer decay time constant of 2.1 ms.

However, for a LIF neuron, between the applied stimulus, the potential of the membrane decays.[34] We use the LIF model to simulate the fabricated artificial neuron based on the double inverter. The threshold fire level in Figure 2 is defined when V_{OUT2} reaches $V_{DD}/2$. The decay of the output voltage from a double inverter can be simply modeled with a first-order Resistance-Capacitance (RC) network.[35]

$$V_{OUT}(t) = V_{DD}e^{\frac{-t}{\tau}} + V_0 \quad (1)$$

where $\tau = RC$. Due to the ambipolar behavior, the low output does not reach zero.[28,36,37] Thus, a V_0 is added in Equation 1. As shown in Figure 2e, the decay of V_{OUT2} can be perfectly fitted with Equation 1, with a time constant of $\tau = 1.4$ ms. The decay value is comparable to the typical decay time (≈10 ms) of the membrane potential in biological thalamic neurons.[38]

Increasing the pulse width to 37 µs, with an interval remaining at 24 µs, can change the output signal, as demonstrated in Figure 2f. After the switch from low to high output voltage, V_{OUT2} is saturated. When the input pulses are stopped, V_{OUT2} decreases for a decay time $\tau = 2.1$ ms as fitted to Equation 1. The decay time constant is 46 % longer compared to Figure 2e. The longer input pulses in Figure 2f result in stronger ferroelectric remanent polarization of the gate oxide in the double inverter, thereby creating more substantial memory effects. The saturation of the domain polarization causes V_{OUT2} saturation. This behavior is similar to the biological thalamic neuron, in which stronger input stimuli increase the recovery time constant.[38]

2.3. Artificial Thalamic Relay Neuron

The double inverter stores the neuron's membrane potential in the soma. In biology, for spike generation, when the potential in the soma reaches a certain threshold, a spike is generated in the axon hillock and transmitted to other neurons via the axon and

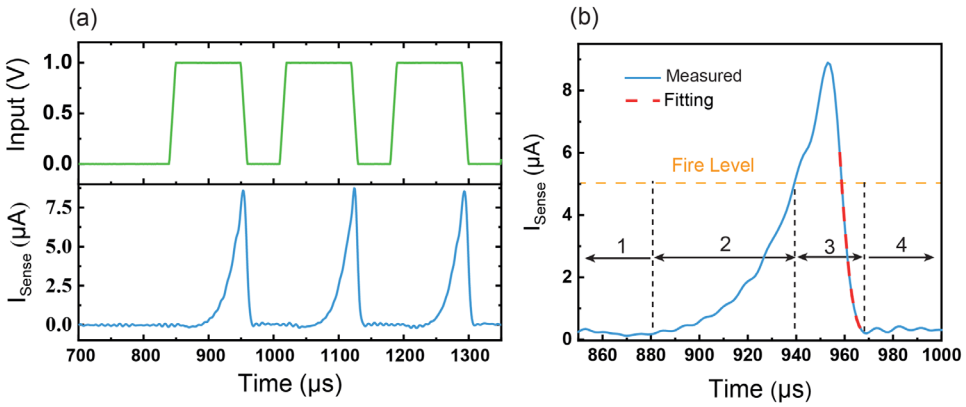

Figure 3. a) Pulses with a width of 100 μs applied at the input of Inverter 1 (top) generate I_{Sense} spikes, corresponding to spikes generated in the Axon Hillock for a biological neuron. The neuron self-resets during the 50μs-long interval. b) Zoom of the first spike in a), showing four different regimes: 1. Resting-state; 2. Integration; 3. Fire, and 4. Self-reset. The decay in I_{Sense} can be fitted using Equation 2 with a time constant of 12 μs.

synapses.[15,18] This operation is performed by T5, which works as a sensing device. In the following, we show the neuron results with the addition of the sensing device T5. In addition to the functions of the LIF-neuron, the neuron exhibits the functions of the thalamic relay neuron.

As previously shown, the applied voltage at the input of Inverter 1 is integrated, resulting in an increased V_{OUT2}. When V_{OUT2} reaches the threshold voltage of T5, a spike is generated in the drain current of T5 (I_{Sense}), as shown in **Figure 3**. When applying a single excitatory input pulse as a stimulus for generating a spike, the length and amplitude of the pulse are the modulation factors that determine whether a spike is generated. Figure 3a shows the generated spikes of T5 by applying input pulses with a pulse width of 100 μs and an amplitude 1 V as stimuli to the artificial neuron. The generated spikes have a frequency of 6.3 kHz. All spikes generated during the measurement are shown in Figure S4a (Supporting Information). Different from Figure 2b where the output is voltage spikes, here the output from T5 is current. We define the fire threshold level as half of the generated peak current. With this definition, the fire threshold in Figure 3 is 5 μA, and the neuron can self-reset during a 50 μs-long pulse interval.

To better understand the neuron function, we focus on a single spike, as indicated by Figure 3b. Four regimes can be defined: resting, integration, firing, and self-resetting. In the first regime of resting (regime 1 in Figure 3b), there is no applied stimulus, and the I_{Sense} is constant. When the stimulus is applied, the current decreases slowly to a minimum and then increases gradually. This is because T2 is turned off slightly more by hole depletion with increased input voltage before an inversion layer is created in the channel. Thus, V_{OUT1} slightly increases, leading to a reduction of V_{OUT2} and I_{Sense}. This corresponds to regime 2 of integration. During the integration, an increasing number of ferroelectric domains in the gate oxides of T1-4 are switching remnant polarization. When the total remnant polarization reaches the level that generates the threshold voltage for T5 in V_{OUT2}, the integration phase transitions into the firing phase, and a spike is generated in I_{Sense}. As the input spike reaches 0 V, the neuron starts the resetting phase (regime 4).

Similar to a single Fe-SBFET synapse, the resetting decay can be fitted with the following equation:[39]

$$I_{Sense} \propto \exp\left(-\frac{4\pi\sqrt{\epsilon_s m^*}}{h}\frac{\varnothing_B}{\sqrt{P_0}}\exp\left[\left(\frac{t}{t_0}\right)^{\frac{n}{2}}\right]\right) \quad (2)$$

where t is the time after the removal of the input spike, ϵ_s The dielectric constant of the semiconductor in the channel,$\varnothing_B$ is the Schottky barrier between the source and semiconductor, P_0 The initial polarization of the ferroelectric material, n is a constant depending on the dimensions of the ferroelectric domains, and t_0 The characteristic time constant. We obtained $t_0 = 12$ μs from the fitting results (Figure 3b and Figure S4b, Supporting Information). Since Equation 2 is only valid after the applied voltage on the gate has been removed, the successful fitting indicates the memory effect. These spike timing characteristics, with a minimum self-reset time of ≈10 μs, make it possible to achieve a frequency of 8.3 kHz with shorter 10 μs pulse intervals compared to Figure 3, as shown in Figure S5 (Supporting Information). Although the frequency can be increased with a lowered fire threshold, the spike height would decrease since the integration regime would be shorter.

The response of T5 depends on the input spikes. For shorter spikes with an amplitude of 1.0 V, a duration of 20 μs, and a 15 μs interval, we achieve tonic spiking from T5, as demonstrated in **Figure 4a**, where the V_{DD} for the inverters and V_{READ} for T5 are 3.0 and 2.0 V, respectively. I_{Sense} remains at a low level after input starts. However, after nine input pulses, a neuron spike is suddenly generated, lasting for two pulses. Subsequently, I_{Sense} drops back to the pre-spike level as the neuron resets during the 15 μs-long pulse intervals. Due to the stochastic nature of Fe-SBFET devices, additional input pulses do not immediately lead to new spikes.[24]

One of the essential properties of thalamic neurons is their function of integrate-or-fire-or-burst (IFB), an extension of the LIF model. The model includes the option of bursting under certain conditions rather than only generating single tonic spikes, allowing for a more accurate simulation of some neurons.[40] The effect is a possible shift in the spiking mode from tonic to

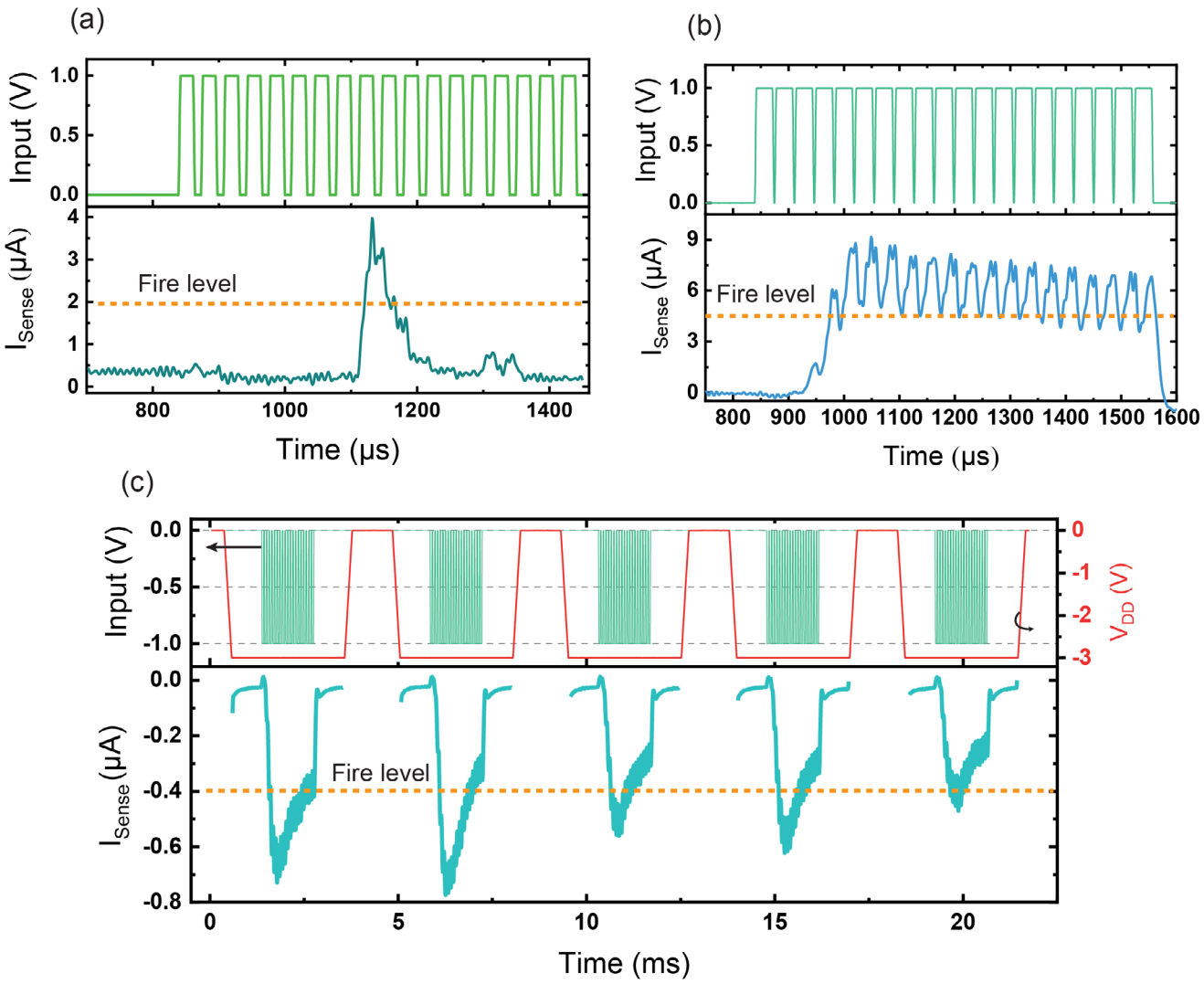

Figure 4. a) The neuron operates in tonic spiking mode, when the pulse train with a longer interval is applied at the input (top). b) A shorter interval at the input results in a burst of spikes instead of single tonic spikes. The neuron is operating in the burst mode. c) The generation of negative spikes in I_{Sense}, demonstrating the operation of the inhibitory neuron.

bursting, which occurs if the biological thalamic neuron is hyperpolarized for a specific time. Thus, the resting potential is moved closer to the threshold voltage for spike generation. Therefore, any further stimuli of the neuron will trigger a burst of spikes.[6]

The burst spiking function of a thalamic neuron can be realized by modulating the stimulus pulses with shorter intervals, as indicated in Figure 4b, where V_{DD}, V_{READ}, and the pulse length are the same as in Figure 4a, although with shorter 5 μs long intervals. When the first two pulses are applied at the input, I_{Sense} remains low. However, a slight increase in current is generated in the I_{Sense} after the third pulse. Subsequent pulses generate spikes with increasing amplitude. After reaching a maximum spike amplitude of 9 μA, resulting in a firing threshold level of 4.5 μA, the following generated spikes show stagnation or degradation in amplitude due to saturation of the neuron. This is because more positive pulses applied on the gate of T1 cause an inversion of the channel, resulting in increased conductance of T1, which increases V_{OUT1} and decreases V_{OUT2}, thereby decreasing I_{Sense}. Despite this effect, each applied pulse still creates a spike above the firing threshold, resulting in bursting behavior due to the continued generation of spikes. In conclusion, in addition to the LIF model, the neuron exhibits the bursting behavior of the IFB model if the applied input is strong enough to make the decay constant for the neuron reset larger than the interval time, thereby generating bursts as a thalamic relay neuron.

Signal transmission during burst mode is more noise-resistant than tonic mode, although the latter can transmit signals with higher accuracy. Biological thalamic neurons are active in burst mode during rapid eye movement (REM) sleep. This mechanism is believed to be associated with pattern recognition of misclassified events experienced during wakefulness, with the bursts providing intensive training for classifying these events.[16]

Based on these findings, when multiple short pulses are applied at the input, the neuron's behavior is similar to that of long pulses because of the accumulation of polarized ferroelectric domains after each stimulus input. However, the dynamics become more complex as the time between input stimuli affects the generation of spikes. Therefore, the interval length between the input pulses serves as an additional modulation factor, leading to tonic LIF or LIFB functions as the interval is shorter.

2.4. Excitatory and Inhibitory Neurons

The sensing device operates as an n-FET in the excitatory neuron, with electrons as the neurotransmitters. The output of the neuron corresponds to a positive sensing current. If spikes of the sensing current are converted to positive voltage pulses and applied to the gates of another excitatory neuron, new spikes can be generated in the other neuron. However, a negative reset spike can speed up the reset process of ferroelectric domains or cancel out the effect of positive voltage pulses. Therefore, the negative sensing current can be the output from an inhibitory neuron. It can subsequently be converted to negative voltage pulses to inhibit the function of excitatory neurons. In the case of the inhibitory artificial neuron, to conserve the symmetry in the neuron circuit and fully function, it is necessary to switch the polarity of all the applied voltages to the neuron.

In Figure 4c, with a fire level of −0.4 μA, the inhibitory neuron behavior is demonstrated with a V_{DD} = −3.0 V and V_{READ} = -1.5 V, where the applied stimuli are negative values. In the initial state, the high negative V_{DD} results in T1 operating as an n-FeFET and T2 being in the off-state. The negative applied input pulses gradually switch the ferroelectric domains in the first inverter. T5 operates in the accumulation region as a p-FET, with holes as neurotransmitters. The Fe-SBFETs in the circuit operate with opposite charge carriers during the integration and firing regimes compared to the same Fe-SBFET in the excitatory neurons. Therefore, the ambipolar characteristics of the Fe-SBFETs are necessary to form neuron circuits that could behave as either inhibitory or excitatory without adjusting the physical circuit.

2.5. Modulation Factors for Stochastic Spiking

One fundamental issue with deterministic neurons is that, according to the Nyquist-Shannon theorem, their firing frequency must exceed twice the external signal frequency to represent information accurately.[41] However, by utilizing probabilistic firing patterns, stochastic neurons offer a different approach that can help relax the strict requirements of deterministic sampling.[42] Furthermore, stochastic neurons can be used for machine learning with the Restricted Boltzmann Machine.[43,44] Key factors affecting the generation of spikes in our neuron include the stimulus amplitude, pulse width, interval between pulses, and the number of pulses. We study the stochastic impact of these factors on the generation of spikes by using a spike probability definition for stochastic artificial neurons.[44] The probability of I_{Sense} that exceeds the set fire level of 1 μA at a V_{READ} = 2 V for T5 is extracted from measurements. The spiking probability is calculated as the number of spikes above the firing level divided by the number of input pulses, as illustrated in Figure S6 (Supporting Information).

The impact of the modulation factors can be seen in **Figure 5**a, where the input pulse amplitude remains constant, and in Figure 5b, where the pulse duration is kept the same. The probability of generating a spike increases as the pulse width increases and the interval between pulses decreases, as indicated in Figure 5a. An increase in amplitude significantly affects the probability of a spike occurring, with a 1 V in amplitude and 100 μs in pulse width reaching 1 in the probability of generating spikes. Conversely, at an amplitude of 0.5 V, the probability of generating a spike is close to 0, even with a short interval, as shown in Figure 5b. This demonstrates a threshold effect on the input voltage required for spike generation. A low voltage pulse below the threshold cannot generate spikes even if applied for a long time. Additionally, it is shown that a longer interval between the applied pulses at the input results in a lower probability of generating a spike. The impact of the interval on the probability of spike generation indicates that this neuron exhibits a leaky effect since the neuron has time to recover its potential if the time between input pulses is too long. Thereby, there is less probability for the spike to be generated.

3. Discussion

The artificial relay neuron presented in this work requires only 4 Fe-SBFETs to simulate the somatic potential and the behavior of the LIF-neuron and 5 Fe-SBFETs to simulate the characteristics of the thalamic neuron. When benchmarking with other state-of-the-art artificial neurons (**Table 1**), this artificial neuron performs well in terms of key metrics for neuromorphic computing. Its fast self-reset enables it to produce spikes at a higher frequency compared to other artificial neurons. Additionally, the effective operation of the inverters resulted in lower energy consumption per spike (40 pJ on average), particularly for the LIF-neuron. The power consumption is ≈50% lower compared to an IF CMOS neuron fabricated with 180 nm technology [22], which consists of complex components such as capacitors, an integrator, and a comparator. Moreover, the scalability of our devices, combined with the reduced number of required transistors, offers significant potential for even lower power consumption and improved area efficiency. Furthermore, the thalamic relay neurons show more functionalities than other neurons, with their ability to adjust their output and generate either tonic or burst spikes based on input.

The similarities in operation to the biological thalamic neuron make it feasible that there are plenty of potential future applications. These applications include relays in brain-machine interfaces for paralyzed people to help connect with bionic limbs. In addition, these artificial thalamic relay neurons can be used as a tool for running real-time simulations to model this part of the brain and its connection with other cortical areas. Meanwhile, they can simultaneously provide enough details on the cellular level, a challenge that even contemporary supercomputers find difficult.[3,4] An increased understanding of the brain could be useful for medical applications, providing insight into how to utilize artificial neurons most effectively. Furthermore, the artificial neuron's stochastic prop-

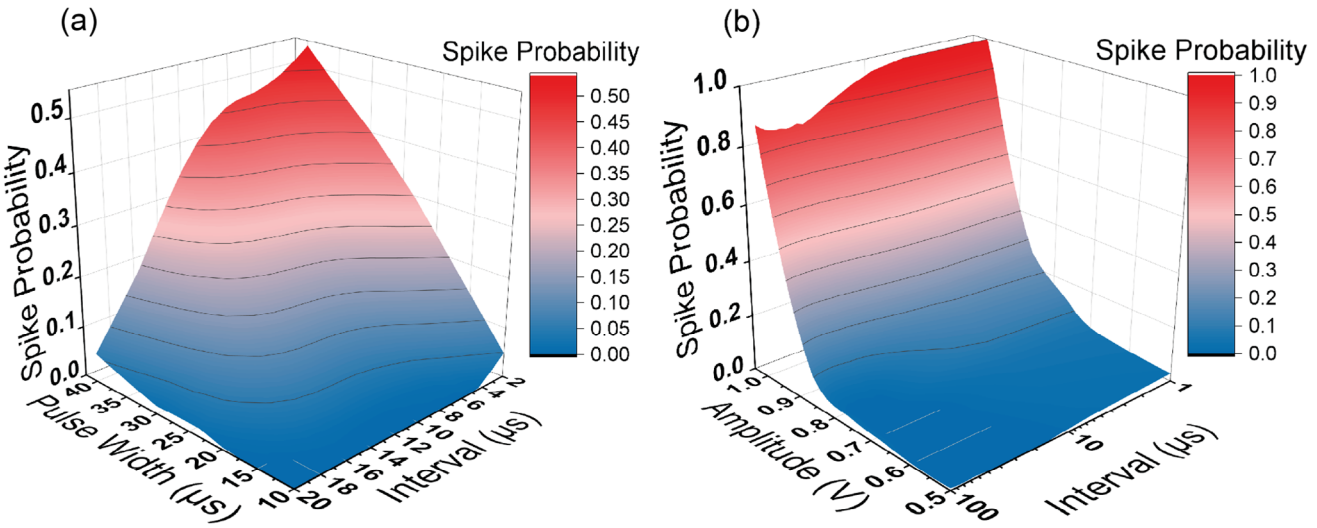

Figure 5. a) Spike probability measured from 40 identical applied voltage pulses at the input with a constant voltage amplitude of 1.0 V. b) Spike probability distribution for input pulses with a constant pulse width of 100 µs.

erties make it suitable for various stochastic-based computing paradigms.

4. Conclusion

To summarize, in this work, artificial stochastic thalamic relay neurons have been demonstrated using Fe-SBFETs. The single Fe-SBFET device can work as a synapse. A double inverter with four identical Fe-SBFETs or with an additional sensing Fe-SBFET can achieve different neuron functionalities of LIF and LIFB depending on the input spikes, demonstrating the properties of the biological thalamic neuron. They consume low energy, on average, 40 pJ per spike for the LIF-neuron, and can operate with a frequency of at least 8.3 kHz. The complete CMOS technology with only 4–5 transistors provides a high potential for large integration and low power consumption. Their applications are not limited to neuromorphic computing, they can also be used for running real-time simulations of the brain for medical applications and brain-machine interfaces. Meanwhile, the relay neuron opens the door to more advanced systems, where various artificial neurons with distinct properties can be interconnected and work together, mimicking the biological brain.

5. Experimental Section

Fabrication of a Single Device: Fe-SBFETs were fabricated on SOI wafers with a top silicon layer of 26 nm. The Mesa pattern was etched with dry etching using SF_6 and O_2. After that, a Nickel layer was sputtered with a thickness of 2.8 nm on top of the Mesa and the surrounding area, with a 4-long gap in the gate region. It was subsequently annealed in forming-gas (90% N_2:10% H_2) for 30s using RTP at 800 °C to form single crystalline $NiSi_2$. The remaining Nickel was removed using Piranha solution (H_2SO_4 1:2 H_2O_2). Then, 11 nm $Hf_{0.5}Zr_{0.5}O_2$ (HZO) was deposited using ALD followed by 40 nm sputtered Titanium Nitride (TiN). This was followed by RTP at 550 C° for 30 s in N_2 to crystallize the HZO into a ferroelectric phase. The TiN gate was patterned with reactive ion etching using Cl_2/Ar plasma, followed by etching of the HZO using CHF_3/Ar plasma and wet etching using Hydrogen Fluoride (HF). The resulting device structure for a single device is illustrated in Figure 2a. Subsequently, a passivation SiO_2 layer was deposited using PECVD, and vias were etched with dry etching, followed by aluminum deposition to form contacts.

Fabrication of Neuron Circuit: Figure S2 (Supporting Information) shows the neuron-integrated circuits' mesa pattern (light gray area). Each inverter pair of devices shares one Mesa structure with a common source area in the center. All the steps of this process were the same as for the fabrication of single devices.

Measurements: The polarization of the ferroelectric HZO was measured using a TF Analyzer 2000 with positive up negative down (PUND) measurement. The devices and artificial neurons were measured using

Table 1. A comparison of the prominent figures of merit for an artificial neuron highlights the differences between the different technologies and this work.

	This Work	Ref. [19]	Ref. [25]	Ref. [47]	Ref. [45]	Ref. [46]	Ref. [21]
Technology	Ferroelectric	Redox	Ferroelectric	Phase-Change	Redox	2D Material	180 nm CMOS
Structure	Fe-SBFET	Ag/SiO_2	FeFET	$Au/VO_2/Au$	$Pt/TiO_x/Ti$	$Li+/MoS_2/Si^+$	MOSFET
Energy/Spike	40 pJ	500 nJ	≈420 pJ	9 nJ	16 nJ	10 nJ	77.24 pJ
Hardware	4/5 Fe-SBFET	1C+2T+1R	2T+1FeFET+1R	1T + 1PCM	1C + 1R	1T: Electrolyte	1C+3R+CMOS
Frequency	8.3 kHz	100 Hz	100 Hz	2.2 kHz	3.2 kHz	20 Hz	330 kHz
Self-reset	Yes	Yes	Yes	Yes	Yes	Yes	No
On/Off Ratio	250	10^6	4	2.75	2	90	10^3
Function	LIF/LIFB	IF	LIF	Oscillatory	LIF	LIF/Clock	IF

a Keithley 4200A-SCS Parameter Analyzer with either Source-Measure units to perform DC-sweep measurement or 4225-PMU pulse measure units for pulse measurements. The PMU was used to read the current spikes generated by the artificial neuron. A DLPCA-200 variable gain low noise current amplifier connected to a Tektronix DPO70604C digital phosphor oscilloscope recorded the somatic potential during high-frequency measurements.

Supporting Information

Supporting Information is available from the Wiley Online Library or from the author.

Acknowledgements

This work was partially supported by the Federal Ministry of Education and Research (BMBF, Germany) in the project NEUROTEC (16ME0398K). This work was performed at Helmholtz Nanofacility (HNF) at Forschungszentrum Juelich.

Open access funding enabled and organized by Projekt DEAL.

Conflict of Interest

The authors declare no conflict of interest.

Data Availability Statement

The data that support the findings of this study are available from the corresponding author upon reasonable request.

Keywords

artificial synapse, ferroelectric, relay, schottky barrier transistor, thalamic neuron

Received: January 7, 2025
Revised: March 7, 2025
Published online: April 25, 2025

[1] D. Arias, S. Saxena, S. E. Verguet, *EClinicalMedicine* **2022**, *54*, 101675.
[2] W. M. Carroll, *Lancet Publishing Group* **2019**, *18*, 418.
[3] G. Indiveri, B. Linares-Barranco, T. J. Hamilton, A. van Schaik, R. Etienne-Cummings, T. Delbruck, S.-C. Liu, P. Dudek, P. Häfliger, S. Renaud, J. Schemmel, G. Cauwenberghs, J. Arthur, K. Hynna, F. Folowosele, S. SAÏGHI, T. Serrano-Gotarredona, J. Wijekoon, Y. Wang, K. Boahen, *Front Neurosci* **2011**, *5*.
[4] H. Liu, Y. Qin, H. Y. Chen, J. Wu, J. Ma, Z. Du, N. Wang, J. Zou, S. Lin, X. Zhang, Y. Zhang, H. Wang, *Adv. Mater.* **2023**, *35*, 2205047.
[5] M. Alawad, M. Lin, *IEEE Trans Emerg Top Comput* **2019**, *7*, 98.
[6] N. a. Lesica, C. Weng, J. Jin, C. I. Yeh, J. M. Alonso, G. B. Stanley, *PLoS Biol.* **2006**, *4*, 1201.
[7] P. Y. Borden, N. C. Wright, A. E. Morrissette, D. Jaeger, B. Haider, G. B. Stanley, *Neuron* **2022**, *110*, 2836.
[8] K. M. Hynna, K. Boahen, *IEEE Trans. Biomed. Eng.* **2009**, *56*, 1734.
[9] M. Wolff, S. Morceau, R. Folkard, J. Martin-Cortecero, a. Groh, *Neurosci Biobehav Rev* **2021**, *120*, 222.
[10] M. J. Redinbaugh, J. M. Phillips, N. Kambi, S. Mohanta, S. Andryk, G. L. Dooley, M. Afrasiabi, A. Raz, Y. B. Saalmann, *Neuron* **2020**, *106*, 66.
[11] S. L. Palay, C. Sotelo, a. Peters, P. M. Orkand, *J. Cell Biol.* **1968**, *38*, 193.
[12] R. Vardi, Y. Tugendhaft, I. Kanter, *Physica A: Statistical Mechanics and its Applications* **2023**, *632*, 129351.
[13] R. K. Wong, M. Stewart, *J Physiol* **1992**, *457*, 675.
[14] R. B. Robinson, S. a. Siegelbaum, *Annu. Rev. Physiol.* **2003**, *65*, 453.
[15] E. M. Izhikevich, J. a. Gally, G. M. Edelman, *Cerebral Cortex* **2004**, *14*, 933.
[16] M. Jändel, 2009 4th International IEEE/EMBS Conference on Neural Engineering, NER '09, IEEE, Antalya, Turkey, June **2009**.
[17] B. W. Connors, M. J. Gutnick, D. a. Prince, *J Neurophysiol* **1982**, *48*, 1302.
[18] T. Guo, K. Pan, B. Sun, L. Wei, Y. Yan, Y. N. Zhou, Y. a. Wu, *Mater. Today Adv.* **2021**, *12*, 100192.
[19] X. Zhang, W. Wang, Q. Liu, X. Zhao, J. Wei, R. Cao, Z. Yao, X. Zhu, F. Zhang, H. Lv, S. Long, M. Liu, *IEEE Electron Device Lett.* **2018**, *39*, 308.
[20] A. Van Schaik, E. Fragnikre, E. Vittoz, *Microelectronics for Neural Networks* **1996**, *1996*, 52.
[21] J. Kim, J. N. Kim, Y. Kim, S. Hwang, M. Koo, *Advanced Intelligent Systems* **2024**, *6*, 1.
[22] S. I. Shkuratov, C. S. Lynch, *Journal of Materiomics* **2022**, *8*, 739.
[23] S. Luo, Y. He, C. Fang, B. Cai, X. Gong, G. Liang, *Jpn. J. Appl. Phys.* **2024**, *63*, 02SP77.
[24] E. Covi, H. Mulaosmanovic, B. Max, S. Slesazeck, T. Mikolajick, *Neuromorphic Computing and Engineering* **2022**, *2*, 012002.
[25] J. Luo, S. Wu, Q. Huang, R. Huang, L. Yu, T. Liu, M. Yang, Z. Fu, Z. Liang, L. Chen, C. Chen, S. Liu, Technical Digest - International Electron Devices Meeting, IEDM 2019, 2019-Decem,6.4.1.
[26] H. Mulaosmanovic, E. Chicca, M. Bertele, T. Mikolajick, S. Slesazeck, *Nanoscale* **2018**, *10*, 21755.
[27] R. Cao, X. Zhang, S. Liu, J. Lu, Y. Wang, H. Jiang, Y. Yang, Y. Sun, W. Wei, J. Wang, H. Xu, Q. Li, Q. Liu, *Nat. Commun.* **2022**, *13*, 1.
[28] R. B. Rashid, W. Du, S. Griggs, I. P. Maria, I. McCulloch, J. Rivnay, *Sci. Adv.* **2021**, *7*, 1.
[29] S. L. Smith, I. T. Smith, T. Branco, M. Häusser, *Nature* **2013**, *503*, 115.
[30] A. Gruverman, H. Tokumoto, A. S. Prakash, S. Aggarwal, B. Yang, M. Wuttig, R. Ramesh, O. Auciello, T. Venkatesan, *Appl. Phys. Lett.* **1997**, *71*, 3492.
[31] F. Xi, Y. Han, M. Liu, J. H. Bae, A. Tiedemann, D. Grützmacher, Q. T. Zhao, *ACS Appl. Mater. Interfaces* **2021**, *13*, 32005.
[32] J. Feng, *Neural Networks* **2001**, *14*, 955.
[33] J. Misra, I. Saha, *Neurocomputing* **2010**, *74*, 239.
[34] M. J. Rozenberg, O. Schneegans, P. Stoliar, *Sci. Rep.* **2019**, *9*, 11123.
[35] L. M. Brocco, S. P. Mccormick, J. Allen, *IEEE Tran. Computer-Aided Design.* **1988**, *7*, 1237.
[36] G. V. Luong, K. Narimani, A. T. Tiedemann, P. Bernardy, S. Trellenkamp, Q. T. Zhao, S. Mantl, *IEEE Electron Device Lett.* **2016**, *37*, 950.
[37] G. V. Luong, S. Strangio, A. T. Tiedemann, P. Bernardy, S. Trellenkamp, P. Palestri, S. Mantl, Q. T. Zhao, *IEEE J. Electron Devices Soc.* **2018**, *6*, 1033.
[38] X. J. Wang, J. Rinzel, M. a. Rogawski, *J Neurophysiol* **1991**, *66*, 839.
[39] F. Xi, A. Grenmyr, J. Zhang, Y. Han, J. H. Bae, D. Grützmacher, Q. T. Zhao, *Adv. Electron. Mater.* **2023**, *9*, 1.
[40] E. M. Izhikevich, *IEEE Trans Neural Netw* **2004**, *15*, 1063.
[41] M. Mishali, Y. C. Eldar, *IEEE Signal Process Mag* **2011**, *28*, 98.
[42] T. Tuma, A. Pantazi, M. Le Gallo, A. Sebastian, E. Eleftheriou, *Nat. Nanotechnol.* **2016**, *11*, 693.
[43] J. Heo, S. Kim, S. Kim, M. H. Kim, *Adv.Sci.* **2024**, *11*, 2405768.

[44] S. Im, J. Hwang, J.-S. Jeong, H. Lee, M. H. Park, J. H. Cho, H. Ju, S. Lee, *Chaos, Solitons and Fractals.* **2024**, *186*, 115195.
[45] S. O. Park, H. Jeong, J. Park, J. Bae, S. Choi, *Nat. Commun.* **2022**, *13*, 1.
[46] L. Bao, J. Zhu, Z. Yu, R. Jia, Q. Cai, Z. Wang, L. Xu, Y. Wu, Y. Yang, Y. Cai, R. Huang, *ACS Appl. Mater. Interfaces* **2019**, *11*, 41482.
[47] E. Corti, A. Khanna, K. Niang, J. Robertson, K. E. Moselund, B. Gotsmann, S. Datta, S. Karg, *IEEE Electron Device Lett.* **2020**, *41*, 629.